Chemical Physics Letters 868 (2025) 142022

Contents lists available at ScienceDirect

Chemical Physics Letters

journal homepage: www.elsevier.com/locate/cplett

Structural, electronic, optical, and magnetic properties of $NbFePb_2O_6$ ferromagnetic semiconductor double perovskite compound

Mohammed Elamin Ketfi [a,*], Saber Saad Essaoud [b,c], Anas Y. Al-Reyahi [d], Said M. Al Azar [e]

[a] Department of Electronics, Faculty of Technology, University of M'sila, University Pole, Road Bordj Bou Arreridj, M'sila28000, Algeria
[b] Department of Physics, Faculty of Sciences, University of M'sila, University Pole, Road Bordj Bou Arreridj, M'sila, 28000, Algeria
[c] Laboratory of materials and renewable energy, Faculty of science, University of M'sila, PO, Box 166 Ichebilia, 28000 M'sila, Algeria
[d] Department of Physics, Faculty of Science, The Hashemite University, P. O. Box 330127, Zarqa 13133, Jordan
[e] Department of Physics, Faculty of Science, Zarqa University, Zarqa 13132, Jordan

ARTICLE INFO

Keywords:
Double perovskites
DFT
Ferromagnetic arrangement
TB-mBJ
Optical absorption

ABSTRACT

This work investigates the magnetic stability, structural, electronic and optical properties of the double perovskite compound $NbFePb_2O_6$.The PBE-GGA function is used to evaluate the structural parameters and verify the magnetic stability among ferromagnetic, paramagnetic and antiferromagnetic states. The compound exhibits ferromagnetic behavior with negative formation enthalpy and positive cohesive energy. The investigation further reveals the compound's semiconducting character with a direct band-gap of 3.40 eV (L-L) in the spin-up state, and an indirect band-gap of 1.87 eV (Γ-X) in spin-down state. The study extends to the compound's response to light incidence, encompassing the calculation of the real and imaginary parts of the dielectric function, the absorption coefficient, the reflectivity and refractivity coefficients, as well as the optical conductivity. The comprehensive analysis yielded results that underscore the compound's suitability for photovoltaic applications, attributable to its semiconducting nature and the optical properties it exhibits.

1. Introduction

Conventional energy sources, including coal and gas, are fast depleting and expected to be completely depleted by 2050 [1]. Scientists are developing technology to produce renewable energy from natural resources to meet rising demand and limited availability. Thermal waste and solar radiation are being studied as potential alternatives to existing energy sources like fossil fuels. Solar cell technology is a cost-effective renewable energy source due to its high power conversion efficiency (PCE) [2–6].

In order to fully utilize all energy sources in solar and thermoelectric systems, robust, economical, and ecologically friendly solutions are being developed. Studying photovoltaic operation and thermal electric conversion techniques (Seebeck and Peltier effect) is therefore essential [7,8]. Finding appropriate compounds and conducting in-depth investigation to assess their potential for energy conversion is the primary problem.

High power conversion efficiencies can be achieved in solar cells using hybrid perovskites containing both organic and inorganic cations [9,10]. These perovskites' long diffusion length, strong charge carrier mobility, and capacity to alter the band gap with various anions make them perfect for use in solar applications [11]. They are regarded as appropriate for this use because they can achieve high power conversion efficiencies as a result [12–14]. Despite the exceptional properties of these materials, their potential uses are restricted because of their unstable structure and the presence of environmentally dangerous poisonous Pb [15–20].

A wide range of material characteristics could be obtained from double perovskites [21,22]. $A_2BB'X_6$ has a variety of physical attributes and unique qualities. Li, Na, K, Rb, and Cs can replace A and B, trivalent metals (Bi, Sb, Y, In, Sc, Tl, Ga) can occupy B′, and halogen ions can be represented by X [23–25]. Perovskites based on alkali metals have exceptional optical and transport qualities, which make them perfect for use in solar cells and other energy-related applications [26–28].The possibility of lead-free perovskites based on alkali metals has been investigated recently for a variety of uses. Al-Aqtash et al. [29]highlighted the excellent optoelectronic and thermoelectric properties of Cs_2AgXBr_6, where X stands for S, Te, and Se, by an ab-initio investigation. A_2RIrO_6's magnetic susceptibilities (where A = Ba, Sr and R = Lu, Sc, La, Y) show paramagnetic properties as low as 4.5 K [30]. Mössbauer

* Corresponding author.
E-mail address: mohammedelamin.ketfi@univ-msila.dz (M.E. Ketfi).

https://doi.org/10.1016/j.cplett.2025.142022
Received 26 November 2024; Received in revised form 20 February 2025; Accepted 26 February 2025
Available online 8 March 2025

spectroscopy and magnetic susceptibility measurements were employed to investigate the electron distribution and magnetic behavior of A_2FeNbO_6 perovskites. Peaks in magnetic susceptibility were noted at approximately 25 K [31] A_2XReO_6 (A = Ba and X = Mn, Ni) was investigated by Saad et al. [32] for energy conversion applications. Outstanding light-absorbing properties have been demonstrated by the creation, characterization, and demonstration of a stable nanocrystal of $Cs_2CuSbCl_6$ [33]. With a total magnetic moment of 2.0 μB, Sr_2CaOsO_6 demonstrates half-metallic ferromagnetism via TB-mBJ-GGA potential [34].

An ab initio investigation was conducted on the mechanical, magneto-electronic, and thermoelectric properties of cubic double perovskites based on Ba_2MgReO_6 and Ba_2YMoO_6 [35]. A_2LiGaI_6 (A = Cs, Rb) [36] and Rb_2InBiX_6 (X = Cl, Br) [37], two previous theoretical investigations on yttrium-based perovskites, suggest that they may be used for green energy consumption. The physical properties of a number of combinations have been studied, including Cs_2AgSbX_6 (X = Cl, Br, I), Rb_2CuSbX_6 (X = Cl, Br, I), Na_2CuMX_6 (M = Sb, Bi; X = Cl, Br), Cs_2CuBiX_6 (X = Cl, Br, I), and Rb_2XInBr_6 (X = Na, K) [38–42].The results validate the wide-ranging uses of Cs and Rb-based perovskite. The importance of Y and Cu for structural stability and physical characteristics is highlighted in this discussion. The crystal lattice structure is strengthened by the addition of Y and Cu at sites B and B′. Make sure the material's composition and physical state do not change in different situations. The optical and transport properties of the material can be impacted by the addition of Y and Cu.

The development of spintronics devices that use spin instead of charge to transmit, process, and store information [43] was the main reason for studying magnetic compounds in the double perovskite oxide family. This work aims to improve understanding of how the Nb-based double perovskite compound $NbFePb_2O_6$ can be used in solar cells. Certain perovskites are not the subject of any theoretical or experimental investigation at this time. The most effective density-functional theory will be used to analyze the compounds according to their physical characteristics. This current research may provide insightful information for next experiments and simulations.

2. Computational details

For determining the physical properties, the current work used the Wien2k software, which is based on the FP-LAPW method and density functional theory [44]. Structural properties were assessed and optimized using the PBE-GGA approach [45]. For optoelectronic devices to perform properly, accurate band gap estimation is essential. The precision of the band gap is underestimated by the PBE-GGA; yet, precision is crucial for electronic and optical analysis calculations. By using the TB-mBJ potential to modify the band gaps, the entire potential strategy has been changed. Within the reciprocal lattice framework, the input factors G_{max} and ℓ are designated as 12 and 10, correspondingly. Up to eight can be found by multiplying the lowest radius of an atomic sphere (R_{min}) by the largest absolute value of the inverse vector (K_{max}). The self-consistent field (SCF) computations were accomplished using a convergence criterion for the total energy of 10^{-5} Ry. The atomic positions are relaxed using force minimization scheme [46] and were adjusted until the force acting on each atom was less than 5×10^{-4} Ry/Bohr. The integration over the first Brillouin zone (BZ) was replaced by a summation on a selected 10 × 10 × 10 *k*-point mesh. By reducing muffin-tin sphere overlap, an appropriate MT radius makes it possible to calculate electron density and potential precisely. The muffin-tin radii of the atoms constituting the compound under study were 2.0, 1.8, 2.4, and 1.6 (a.u.) for Nb, Fe, Pb, and O, respectively. The optical properties were estimated after calculating the complex dielectric function, indicated as $\varepsilon(\omega)$, which uses to describe response of matter to incident electromagnetic waves, particularly in its linear optical characteristics [47].

3. Results and discussion

3.1. Structural properties

The geometric stability of any compound plays a key part as all the essential properties are based on the stability of the material [48]. The structural configuration provides valuable information for comprehending the precise positioning of atoms inside the unit cell of the crystal's framework. The formula $NbFePb_2O_6$ consists a cubic perovskite with space group Fm3-m (#225) as shown in Fig. 1 through of four separate parts (Nb, Fe, Pb, and O) in a proportion of 1:1:2:6. Within this structure, Nb, Fe, Pb and O atoms occupy 8c (0,0,0), 4a (0.5, 0, 0), 4b (0.25, 0.25, 0.25), and 24e (0.5, 0, x) sites, respectively. Notably, the variable x takes positions at 0.2508 and 0.7491. The optimized lattice parameters is 7.7869 Å.

This determines the exact geometric configuration of the finished materials, assigning each atom to the appropriate spot as needed. Moreover, the periodic or geometric arrangement of atoms offers an even more advantageous opportunity to study the overall ground state energy of these alloys. Several structural characteristics were obtained by fitting the total energy vs. Unit cell volume graph using the Murnaghan equation of state [49]. $NbFePb_2O_6$'s stability is explained by optimization, which brings its atoms closer together and produces the maximum electron density and energy release. The reason for this is that the system would rather keep its potential lower. Basic ideas imply that bond formation is an exothermic process since it releases energy. As seen in Fig. 2, the obtained energy validates that these compound has stable ground state energies, increasing their energetic stability. Furthermore, Table 1 provides information on a number of ground state properties, including bulk modulus B_0 (GPa), lowest energy E_0 (Ry), pressure derivative B′, and volume V_0 ($a.u^3$).

Meanwhile, the cohesion energy and the formation enthalpy are computed using the formula [50], as follows:

$$E_{coh} = \frac{(E_{Nb} + E_{Fe} + 2E_{Pb} + 6E_O) - E_{NbFePb_2O_6}}{10} \quad (1)$$

E_{Nb}, E_{Fe}, E_{Pb}, and E_O denote the energy measurements for the elements Nb, Fe, Pb, and O, respectively, whereas $E_{NbFePb2O6}$ denotes the total computed energy of the material.

Also, The enthalpy of formation (ΔH_{for}) of $NbFePb_2O_6$ in paramagnetic (PM), antiferromagnetic (AFM) and ferromagnetic (FM) states was determined the following expression:

$$\Delta H_{for} = \frac{E_{NbFePb_2O_6} - \left(E^{solid}{}_{Nb} + E^{solid}{}_{Fe} + 2E^{solid}{}_{Pb} + 6E^{Gaz}{}_{O}\right)}{10} \quad (2)$$

$E_{NbFePb_2O_6}$ represents the total energy of the $E_{NbFePb_2O_6}$ unit cell, $E^{solid}{}_{Nb}$ and $E^{solid}{}_{Fe}$ and $E^{solid}{}_{Pb}$ denote the total energies per atom of the solid form of the pure elements Nb, Fe and Pb respectively, whileE^{O}_{Gas} denote the total energies per atom of the gaseous state of the oxygen atom.

From Table 1, the positive values obtained for the cohesive energy of $NbFePb_2O_6$ in the three magnetic states indicate that the ferromagnetic state is more cohesive than the paramagnetic state. In addition, the values obtained for the negatively valued $NbFePb_2O_6$ enabled the thermodynamic stability of the compound to be proven.

In order to ascertain the most stable state for the studied compound, the energy-volume curves for paramagnetic (PM), antiferromagnetic (AFM) and ferromagnetic (FM) states were plotted in Fig. 2. It is evident from the figure that the ferromagnetic state has a lower energy than antiferromagnetic and paramagnetic states.

The microscopic magnetic behavior in matter expresses the quantum exchange interactions which are related to atoms' magnetic moments, the distance between them, and the external magnetic field to which they are subjected [51,52]. These interactions were modeled using the effective spin Hamiltonian of Heisenberg given by:

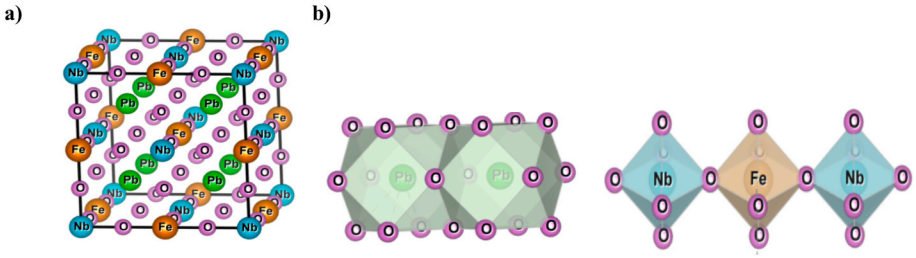

Fig. 1. (a): Crystal Cubic structure of $NbFePb_2O_6$ compound, **(b):** Polyhedral view along an axis.

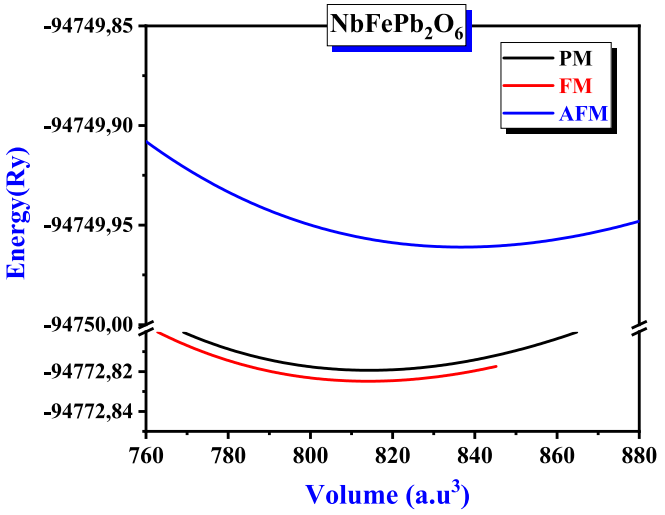

Fig. 2. Total energy versus volume calculated using GGA functional for $NbFePb_2O_6$.

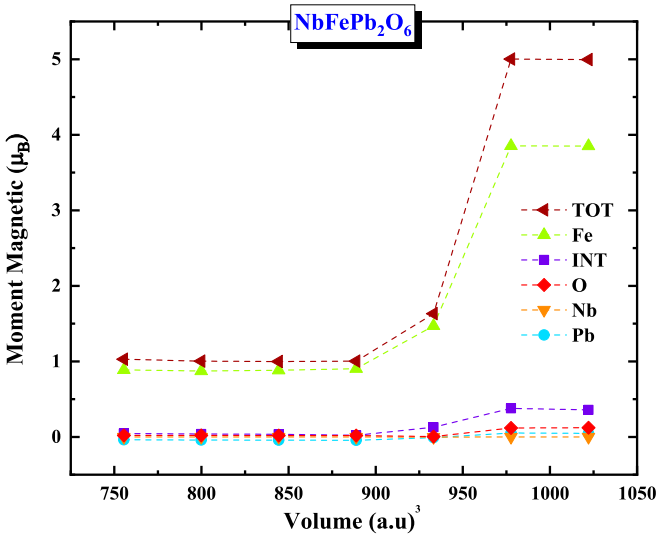

Fig. 3. Total and partial magnetic moment variations as function of volume for $NbFePb_2O_6$.

Table 1
The calculated equilibrium lattice constants, bulk modulus, cohesive energy, and formation enthalpy for $NbFePb_2O_6$ compound obtained by using GGA-PBE approximations in both magnetic states (PM and FM).

	a (Å)	B(GPa)	E_{coh}(eV/atom)	ΔH_{for}(eV/atom)
FM	7.787	261.698	5.942	−3.826
PM	7.844	200.911	5.935	−3.811
AFM	7.479	185.468	5.788	−3.671

$$H_{mag} = \sum_{ij} J_{ij} \vec{S}_i . \vec{S}_j + \sum_i g_i \mu_B \vec{h} \vec{S}_i \quad (3)$$

Here, μB is the Bohr magneton, gi is the magnetic ratio, $S^{\rightarrow}i$ is the spin operator, $h^{\rightarrow\rightarrow}$ is the external magnetic field, and Jij is the exchange coupling constant (which depends on the distance between the two atoms).

As shown in Fig. 3, the changes in the total magnetic moment of the compound are clearly affected by the change in volume, as its value decreased from 5 to 1 μ_B due to the change in volume resulting from the compound being subjected to external pressure. This is in contrast to some other compounds that are known to be magnetically stable even under the influence of external pressure, such as Dy_2CoMnO_6 [51], Ba_2MnReO_6, Ba_2NiReO_6 and Sr_2MnReO_6 [32]. The magnetic behavior of this compound can be explained by the magnetic exchange interaction, where by studying the distribution of the density of states of the atomic orbitals in the compound, it becomes clear that the d orbital's of the iron and niobium atoms close to the Fermi level contribute to the excitation and interaction of the electrons in the p orbitals of oxygen due to their presence within a strong internal potential, and the resulting interaction leads to the arrangement of the spins of the electrons in the d orbitals in a parallel manner, which gives the compound a magnetic moment.

3.2. *Electronic properties*

Double perovskite compounds have promising uses in energy conversion, catalysis, and electronic devices. Understanding the electrical properties of double perovskite materials is crucial for improving their functionality and enabling new applications.

The energy band structure of the studied material was calculated at high-symmetry points within the first Brillouin zone. Fig. 4 demonstrates semiconductor, exhibiting a direct band-gap of 3.40 eV (L-L) in the spin-up state and an indirect band-gap of 1.87 eV (Γ-X) in spin-down state.

The analysis of the total and partial state density curves in Fig. 5 validated the conclusions obtained from the energy band structure curves, as we observe in both spin directions, the presence of a bandgap with a zero density of states near the Fermi level, separating the conduction bands from the valence bands. According to Fig. 5, the PDOS curves demonstrate that the electrons of the atoms forming the compound $NbFePb_2O_6$ are distributed as follows: the electrons of the Pb atom have two clear contributions in both spin states where the first is due to the electrons of the s orbital in the energy range [−8 eV; -6 eV] from the valence region and the electrons of the p orbital in the energy range [+5 eV; +8 eV] from the conduction region. In the case of the electrons of the d orbital of the iron atom, the contribution of the electrons in the spin-up state was moderately strong in the formation of the valence bands extending from −7 eV to Fermi level, and strongly significant in the formation of the conduction bands extending from +2 eV, to +4 eV. In the case of the Nb atom, it has been demonstrated that the electrons of the ***d*** orbit contribute effectively to the formation of certain

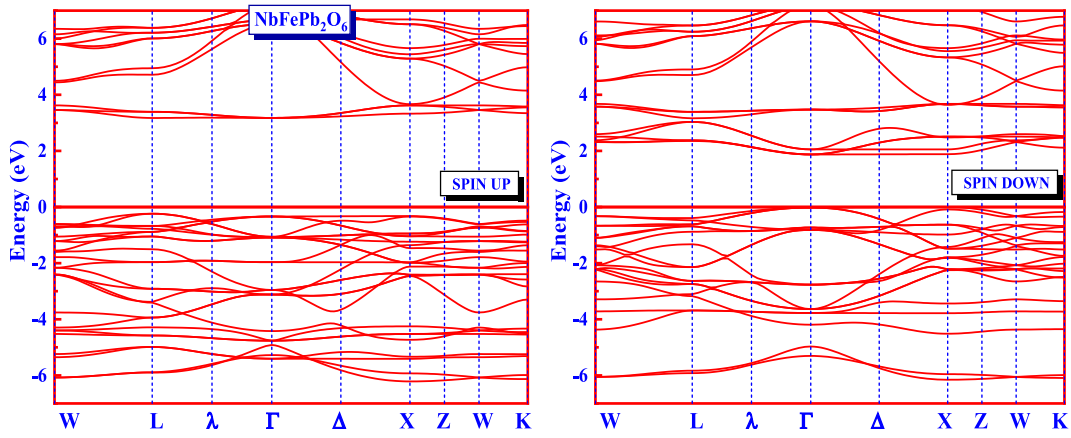

Fig. 4. Band structure curves for $NbFePb_2O_6$ within the TB-mBJ approximation.

conduction bands, which are confined from +3 eV to +4.5 eV. On the other hand, the contribution of the ***p*** orbital electrons of the oxygen atom in both spin states was located at the valence bands in the energy range [−3 eV;0 eV].

We can conclude from the analysis of the atoms' partial density of states curves that the origin of this compound's magnetic behavior is the obvious displacement between the spin-up and spin-down spin states of the partial density of electrons in each of the iron (Fe) and niobium (Nb) atoms'***d*** orbitals. This displacement causes a magnetic moment to be generated as a result of the asymmetry in the distribution of the density of states between spin up and down states, which in turn increases the polarization of electrons in these orbitals.

3.3. Optical properties

The compound's optical characteristics are estimated for photovoltaic applications with photon energies ranging from 0 to 8 eV. The optical properties of a material are determined by its complex dielectric function, which includes both real and imaginary parts [53].

$$\varepsilon = \varepsilon_1(\omega) + \hat{i}\,\varepsilon_2(\omega) \tag{4}$$

Where are $\varepsilon_1$real and $\varepsilon_2$imaginary parts of the dielectric function. The material's degree of polarization under the influence of an external electric field is represented by $\varepsilon_1$whereas the material's absorption behavior is associated with ε_2Fig. 6 shows the computed $\varepsilon_1$and ε_2(values)

The electronic polarizability of the double perovskite compound is revealed by $\varepsilon_1(\omega)$, which also shows how electromagnetic (EM) radiation disperses upon them. The static values for the compound progressively rise to it maximum value at 3.22 eV, indicating that these compound exhibit strong electrical polarization behavior within the visible light range. As photon energy rises, the value is seen to slightly decrease.

The response of the developing electromagnetic radiation on the materials is captured by the $\varepsilon_2\ (\omega)$component, which clarifies state transitions from the unoccupied conduction band to the occupied valence band. High absorption in the visible region is indicated by our compound's $\varepsilon_2\ (\omega)$ peak value, which is observed at 3.38 eV and is followed by a notable reduction in the imaginary part $\varepsilon_2\ (\omega)$ of the dielectric function.

The calculated results for the above mentioned optical parameters are shown in Fig.6 (c) and (d) where presents the curves for the refractive index $n(\omega)$ and extinction coefficient $k(\omega)$ of $NbFePb_2O_6$. The k(ω) represents the dissipation of electromagnetic waves within the material. When the trends of η(ω) and k(ω) for the compound closely follow the trends of their $\varepsilon_1\ (\omega)$ and $\varepsilon_2\ (\omega)$, respectively. This indicates that the calculated results align well with the established relationships between these optical parameters. The static refractive indices $\eta(0)$are 2.96, which correspond to $\varepsilon_1(\omega)$ based on the below mentioned relations [54].

$$\eta(\omega) = \left(\frac{1}{\sqrt{2}}\right)\left[\sqrt{\varepsilon_1{}^2(\omega) + \varepsilon_2{}^2(\omega)} + \varepsilon_1\ (\omega)\right]^{1/2} \tag{5}$$

$$k(\omega) = \left(\frac{1}{\sqrt{2}}\right)\left[\sqrt{\varepsilon_1{}^2(\omega) + \varepsilon_2{}^2(\omega)} - \varepsilon_1\ (\omega)\right]^{1/2} \tag{6}$$

To further understand the optical properties of $NbFePb_2O_6$, other important optical parameters such as the optical absorption coefficient α(ω), conductivity σ(ω) and reflectivity R(ω) can be deduced from $\varepsilon_1(\omega)$ and $\varepsilon_2(\omega)$ using the following Eqs. [55]:

$$\alpha(\omega) = \frac{2\pi\omega}{c}\sqrt{\frac{-R_e(\varepsilon(\omega)|\varepsilon(\omega)|)}{2}} \tag{7}$$

$$\sigma(\omega) = -\left(\frac{i\omega}{4\pi}\right)\varepsilon(\omega) \tag{8}$$

$$R(\omega) = \frac{[n-1]^2 + k^2}{[n+1]^2 + k^2} \tag{9}$$

Additionally, Fig. 7(b) illustrates the $\sigma(\omega)$spectra of the incident photon, which correspond to the conduction of photo-electrons under radiation energy. The $\sigma(\omega)$ of $NbFePb_2O_6$ begins to increase beyond 3.23 eV and reaches a maximum value of $27{,}941.51\Omega^{-1}\,cm^{-1}$ at 3.38 eV. Fig. 7(a) as a function of the incident photon energy displays the varying absorption coefficient $\alpha(\omega)$. Generally, $\alpha(\omega)$ represents the amount of incident light energy absorbed per unit thickness of the material. A higher absorption coefficient value indicates more efficient electron transport from the valence band (VB) to the conduction band (CB). The results demonstrated a broad absorption range from visible (vis) to ultraviolet (UV) light, with a maximum value of 178.66×10^4/cm at 3.38 eV for $NbFePb_2O_6$. By establishing a correlation between the outcomes of the absorption curve and the partial density of states curves (Fig. 5), it becomes evident that the upper absorption peak situated within the energy range of 3.5 to 4 eV can be attributed to the interband excitation of electrons from the p orbital of the oxygen atom to the d orbital of the Nb atom.

Based on Fig. 7(a), $\alpha(\omega)$was nearly zero in the same region where the optical conductivity, $\sigma(\omega)$ was also zero. The findings revealed that $\sigma(\omega)$ reached its maximum value when the absorption was at its peak. In the Fig.6(c), the zero-frequency reflectivity limit of $NbFePb_2O_6$ is found to be 0.25. High reflex peaks are observed 0.83 at energy 3.82 eV for the compound corresponding to the negative values of $\varepsilon_1(\omega)$. Therefore, the results of this study demonstrate the suitability of $NbFePb_2O_6$ for use in vis and UV-based optoelectronic devices.

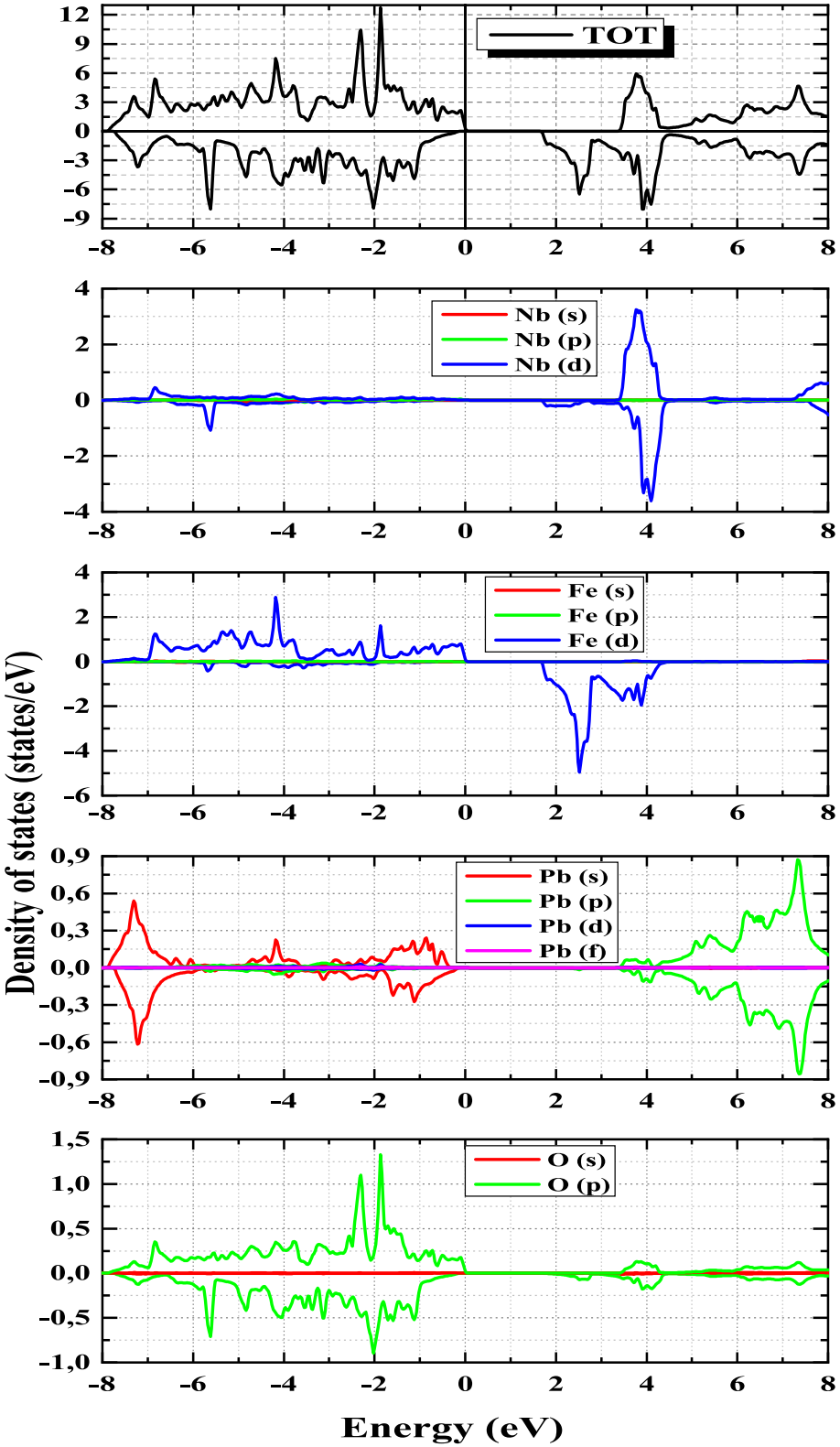

Fig. 5. The calculated total and partial density of states for both $NbFePb_2O_6$within the TB-mBJ approximation.

4. Conclusion

The structural, electronic, optical and magnetic properties of $NbFePb_2O_6$ compound were investigated using ab initio calculations. The structural parameters were optimized using the generalized gradient approximation (PBE) where the stability of the compound in its ferromagnetic phase was confirmed, and its thermodynamic stability was proven by calculating the enthalpy of formation.

The compound in its magnetic phase showed a magnetic moment that increases with the increase in the size of the crystal cell of the compound, and it showed semiconductor behavior in its most stable state with a direct band-gap of 3.40 eV (L-L) in the spin-up state, and an

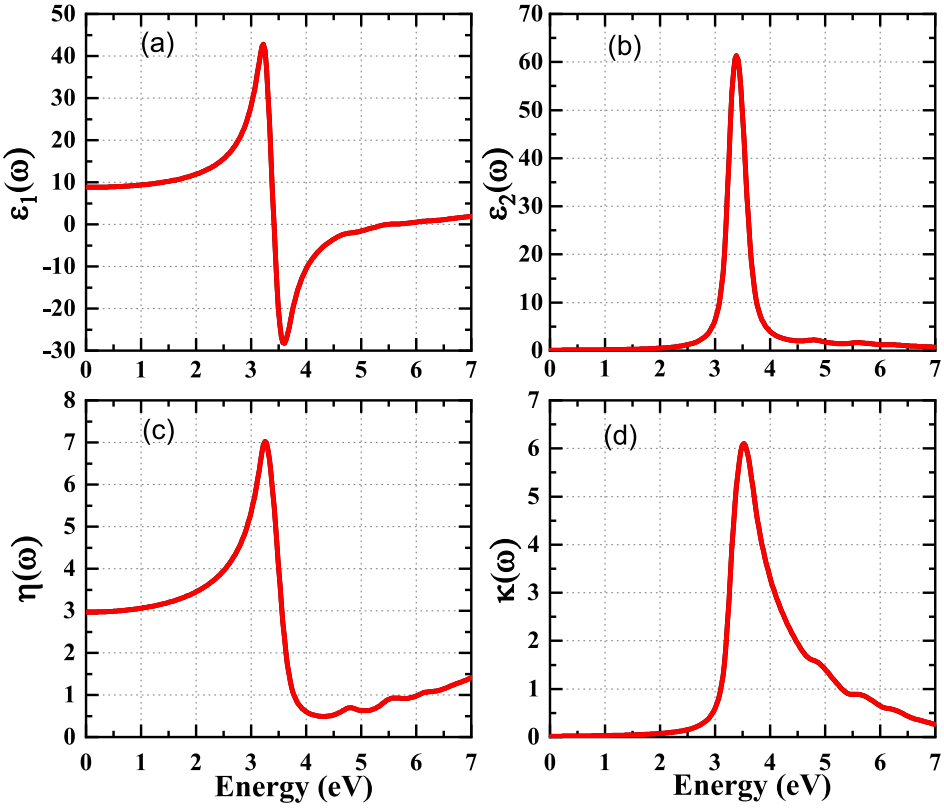

Fig. 6. Estimated $\varepsilon_1(\omega)$ real plot, $\varepsilon_2(\omega)$ imaginary plot of dielectric constant and the computed plot of refractive index $\eta(\omega)$ as well as extinction coefficient $k(\omega)$ for $NbFePb_2O_6$.

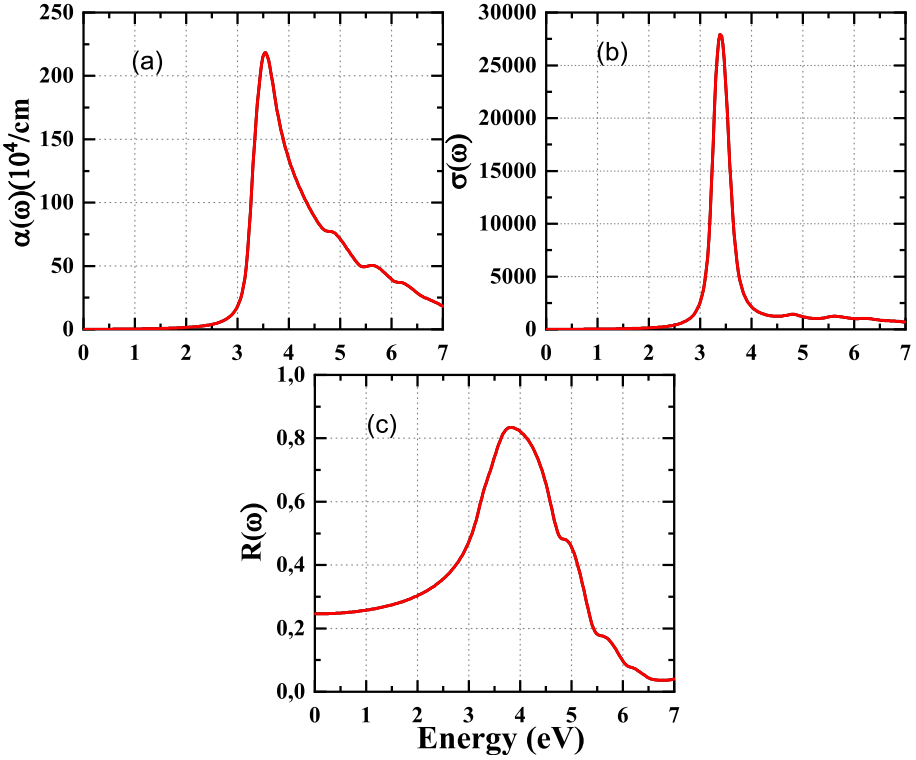

Fig. 7. Optical conductivity $\sigma(\omega)$, Reflectivity $R(\omega)$ and absorption coefficient $\alpha(\omega)$ for $NbFePb_2O_6$.

indirect band-gap of 1.87 eV (Γ-X) in spin-down state.

The response of the compound to the incident electromagnetic radiation was studied, as the compound showed good absorption of light in the visible light range, which is a candidate for being a light detector or sensor.

CRediT authorship contribution statement

Mohammed Elamin Ketfi: Writing – review & editing, Writing – original draft, Visualization, Supervision, Software, Resources, Methodology, Formal analysis, Data curation, Conceptualization. **Saber Saad Essaoud:** Writing – review & editing, Visualization, Supervision, Conceptualization. **Anas Y. Al-Reyahi:** Visualization, Supervision. **Said M. Al Azar:** Visualization, Supervision.

Declaration of competing interest

The authors declare that they have no known competing financial interests or personal relationships that could have appeared to influence the work reported in this paper.

Data availability

Data will be made available on request.

References

[1] N. Abas, A. Kalair, N. Khan, Review of fossil fuels and future energy technologies, Futures 69 (2015) 31–49, https://doi.org/10.1016/j.futures.2015.03.003.

[2] P.A. Owusu, S. Asumadu-Sarkodie, A review of renewable energy sources, sustainability issues and climate change mitigation, Cogent Eng. 3 (2016) 1167990, https://doi.org/10.1080/23311916.2016.1167990.

[3] M. Liu, S. Baisheng, M. Alharthi, M.S. Hassan, I. Hanif, The role of natural resources, clean energy and technology in mitigating carbon emissions in top populated countries, Res. Policy 83 (2023) 103705, https://doi.org/10.1016/j.resourpol.2023.103705.

[4] C.R. Kumar, J.M.A. Majid, Renewable energy for sustainable development in India: current status, future prospects, challenges, employment, and investment opportunities, Energy Sustain. Soc. 10 (2020) 2, https://doi.org/10.1186/s13705-019-0232-1.

[5] J.L. Holechek, H.M.E. Geli, M.N. Sawalhah, R. Valdez, A global assessment: can renewable energy replace fossil fuels by 2050? Sustainability 14 (2022) 4792, https://doi.org/10.3390/su14084792.

[6] J. Werner, L. Barraud, A. Walter, M. Bräuninger, F. Sahli, D. Sacchetto, N. Tétreault, B. Paviet-Salomon, S.-J. Moon, C. Allebé, M. Despeisse, S. Nicolay, S. De Wolf, B. Niesen, C. Ballif, Efficient near-infrared-transparent perovskite solar Cells enabling direct comparison of 4-terminal and monolithic perovskite/silicon tandem Cells, ACS Energy Lett. 1 (2016) 474–480, https://doi.org/10.1021/acsenergylett.6b00254.

[7] M. Benghanem, A.A. Al-Mashraqi, K.O. Daffallah, Performance of solar cells using thermoelectric module in hot sites, Renew. Energy 89 (2016) 51–59, https://doi.org/10.1016/j.renene.2015.12.011.

[8] H. Alghamdi, C. Maduabuchi, K. Okoli, M. Alobaid, M. Alghassab, A.S. Alsafran, E. Makki, M. Alkhedher, Latest advancements in solar photovoltaic-thermoelectric conversion technologies: thermal energy storage using phase change materials, machine learning, and 4E analyses, Int. J. Energy Res. 2024 (2024) 1–29, https://doi.org/10.1155/2024/1050785.

[9] R. Singh, S. Dogra, S. Dixit, N.I. Vatin, R. Bhardwaj, A.K. Sundramoorthy, H.C. S. Perera, S.P. Patole, R.K. Mishra, S. Arya, Advancements in thermoelectric materials for efficient waste heat recovery and renewable energy generation, Hybrid Adv. 5 (2024) 100176, https://doi.org/10.1016/j.hybadv.2024.100176.

[10] Y. Ahmed, B. Khan, M. Bilal Faheem, K. Huang, Y. Gao, J. Yang, Organic additives in all-inorganic perovskite solar cells and modules: from moisture endurance to enhanced efficiency and operational stability, J. Energy Chem. 67 (2022) 361–390, https://doi.org/10.1016/j.jechem.2021.09.047.

[11] R.A. Afre, D. Pugliese, Perovskite solar Cells: a review of the latest advances in materials, Fabrication Techniques, and Stability Enhancement Strategies, Micromachines 15 (2024) 192, https://doi.org/10.3390/mi15020192.

[12] Y.A. Ramirez, A. De La Rosa, C.H. Enriquez, D.A. Rivera, V.M. Rodriguez, A. J. Telles, L.V. Frias, D.R. Hodges, High-Voltage Hybrid Organic-Inorganic Perovskite Solar Cells, IEEE 48th Photovolt. Spec. Conf, PVSC, IEEE, Fort Lauderdale, FL, USA 2021 (2021) 2303–2306, https://doi.org/10.1109/PVSC43889.2021.9518561.

[13] Y. Zhang, A. Kirs, F. Ambroz, C. Lin, A.S.R. Bati, I.P. Parkin, J.G. Shapter, M. Batmunkh, T.J. Macdonald, Ambient Fabrication of Organic–Inorganic Hybrid Perovskite Solar Cells, Small Methods 5 (2021) 2000744, https://doi.org/10.1002/smtd.202000744.

[14] Q. Chen, N. De Marco, Y. Michael Yang, T.-B. Song, C.-C. Chen, H. Zhao, Z. Hong, H. Zhou, Y. Yang, Under the spotlight: the organic–inorganic hybrid halide perovskite for optoelectronic applications, Nano Today 10 (2015) 355–396, https://doi.org/10.1016/j.nantod.2015.04.009.

[15] M.J. Martínez-Lope, J.A. Alonso, M.T. Casais, Synthesis, crystal and magnetic structure of the double perovskites a $_2$ NiMoO $_6$ (a = Sr, Ba): a neutron diffraction study, Eur. J. Inorg. Chem. 2003 (2003) 2839–2844, https://doi.org/10.1002/ejic.200300063.

[16] A.A. Sokan-Adeaga, M.A. Sokan-Adeaga, E.D. Sokan-Adeaga, A.N. Oparaji, H. Edris, E.O. Tella, F.A. Balogun, M. Aledeh, O.E. Amubieya, Environmental toxicants and health adversities: a review on interventions of phytochemicals, J. Public Health Res. 12 (2023), https://doi.org/10.1177/22799036231181226, 22799036231181226.

[17] M. Kibbou, Z. Haman, Z. Lahbi, E. Ouabida, I. Essaoudi, R. Ahuja, A. Ainane, Advancing photovoltaics and optoelectronics: exploring the superior performance of lead-free halide perovskites, Opt. Mater. 147 (2024) 114737, https://doi.org/10.1016/j.optmat.2023.114737.

[18] S.S. Essaoud, S.M. Azar, A.A. Mousa, A.Y. Al-Reyahi, DFT-based investigation of electronic-structure, magnetic and thermoelectric properties of Dy $_2$ CoMnO $_6$ double perovskite, Phys. Scr. 98 (2023) 075930, https://doi.org/10.1088/1402-4896/acdd2c.

[19] N.A. Aqtash, S.M. Al Azar, A.Y. Al-Reyahi, A. Mufleh, M. Maghrabi, S.S. Essaoud, K. Berarma, A.A. Mousa, First-principles calculations to investigate structural, mechanical, electronic, optical, and thermoelectric properties of novel cubic double Perovskites X2AgBiBr6 (X=Li, Na, K, Rb, Cs) for optoelectronic devices, Mol. Simul. 49 (2023) 1561–1572, https://doi.org/10.1080/08927022.2023.2251604.

[20] A. Mera, M. Awais Rehman, Z. Ur Rehman, Z. Sarfraz, M. Sohaib, J. Fatima, M. Usman, Exploring the physical properties of Rb2TlSbM6 (M = cl, Br) inorganic halide perovskites for solar cell applications: a DFT study, Inorg. Chem. Commun. 165 (2024) 112528, https://doi.org/10.1016/j.inoche.2024.112528.

[21] E.T. Chenebuah, M. Nganbe, A.B. Tchagang, Comparative analysis of machine learning approaches on the prediction of the electronic properties of perovskites: a case study of ABX3 and A2BB'X6, Mater. Today Commun. 27 (2021) 102462, https://doi.org/10.1016/j.mtcomm.2021.102462.

[22] I. Vázquez-Fernández, S. Mariotti, O.S. Hutter, M. Birkett, T.D. Veal, T.D. C. Hobson, L.J. Phillips, L. Danos, P.K. Nayak, H.J. Snaith, W. Xie, M.P. Sherburne, M. Asta, K. Durose, Vacancy-ordered double perovskite Cs_2 TeI_6 thin films for optoelectronics, Chem. Mater. 32 (2020) 6676–6684, https://doi.org/10.1021/acs.chemmater.0c02150.

[23] Q. Zhang, F. Hao, J. Li, Y. Zhou, Y. Wei, H. Lin, Perovskite solar cells: must lead be replaced – and can it be done? Sci. Technol. Adv. Mater. 19 (2018) 425–442, https://doi.org/10.1080/14686996.2018.1460176.

[24] B. Huang, G. Frapper, Barium–Nitrogen Phases Under Pressure: Emergence of Structural Diversity and Nitrogen-Rich Compounds, Chem. Mater. 30 (2018) 7623–7636, https://doi.org/10.1021/acs.chemmater.8b02907.

[25] A. Alshoaibi, A.C. Nkele, S.A. Getaneh, C. Awada, S. Islam, F.I. Ezema, Investigating the properties of co-precipitated nickel cobalt phosphate (NiCoP) nanoparticles for energy storage applications, Phys. Scr. 99 (2024) 075984, https://doi.org/10.1088/1402-4896/ad5800.

[26] A.U. Haq, T.S. Ahmad, M. Amin, A. Bakar, A. Afaq, N. Ehsan, S.M. Ramay, A. A. Siddig, A first principle investigation of electronic, mechanical, optical and transport properties of a $_2$ AgAlI $_6$ (a = Rb, K, Na) for energy harvesting, Phys. Scr. 98 (2023) 115972, https://doi.org/10.1088/1402-4896/ad032c.

[27] A. Mera, A. Almeshal, S.A. Rouf, T. Zelai, A.I. Aljameel, O. Hakami, Q. Mahmood, Modification of band gaps by changing anions to optimize the double perovskites K2NaTlX6 (X = cl, Br, I) for solar cells and transport applications, Chem. Phys. Lett. 829 (2023) 140754, https://doi.org/10.1016/j.cplett.2023.140754.

[28] R. Kristian Pingak, A. Harbi, S. Bouhmaidi, F. Nitti, M. Moutaabbid, L. Setti, A. Zicko Johannes, N.U.J. Hauwali, Vacancy-ordered CsRbGeCl6 and CsRbGeBr6 perovskites as new promising non-toxic materials for photovoltaic applications: A DFT investigation, Chem. Phys. 584 (2024) 112348, https://doi.org/10.1016/j.chemphys.2024.112348.

[29] N. Al-Aqtash, A.Y. Al-Reyahi, S. Al Azar, S.S. Essaoud, M. Maghrabi, A. Mufleh, M. E. Ketfi, K. Berarma, An ab-initio study on the physical properties of double perovskite Cs2AgXBr6 (X=S, Te, Se), Mater. Today Commun. 38 (2024) 108222, https://doi.org/10.1016/j.mtcomm.2024.108222.

[30] E.C. Koskelo, N.D. Kelly, L.A.V. Nagle-Cocco, J.D. Bocarsly, P. Mukherjee, C. Liu, Q. Zhang, S.E. Dutton, Magnetic and Magnetocaloric properties of the a $_2$ LnSbO $_6$ lanthanide oxides on the frustrated *fcc* lattice, Inorg. Chem. 62 (2023) 10317–10328, https://doi.org/10.1021/acs.inorgchem.3c01137.

[31] K. Tezuka, K. Henmi, Y. Hinatsu, N.M. Masaki, Magnetic susceptibilities and Mössbauer spectra of perovskites A2FeNbO6 (a=Sr, Ba), J. Solid State Chem. 154 (2000) 591–597, https://doi.org/10.1006/jssc.2000.8900.

[32] S. Saad Essaoud, M.E. Ketfi, S. Al Azar, A.Y. Al-Reyahi, A. Mufleh, Computational study of structural parameters, magnetic properties, half metallicity, and linear optical characteristics of transition-metal oxide double perovskites: Ba2MnReO6, Ba2NiReO6, and Sr2MnReO6, Indian J. Phys. (2024), https://doi.org/10.1007/s12648-024-03264-7.

[33] T.-Y. Tang, Y.-L. Tang, Physical and optoelectronic properties of double halide perovskites A2CuSbX6 (a = Cs, Rb, K; X = cl, Br, I) based on first principles calculations, Chem. Phys. 570 (2023) 111897, https://doi.org/10.1016/j.chemphys.2023.111897.

[34] S. Haid, B. Bouadjemi, M. Houari, M. Matougui, T. Lantri, S. Bentata, Z. Aziz, Optical properties of half-metallic ferrimagnetic double perovskite Sr2CaOsO6

compound, Solid State Commun. 322 (2020) 114052, https://doi.org/10.1016/j.ssc.2020.114052.
[35] M.E. Ketfi, S.S. Essaoud, S.M. Al Azar, A.Y. Al-Reyahi, A.A. Mousa, N. Al-Aqtash, Mechanical, magneto-electronic and thermoelectric properties of Ba $_2$ MgReO $_6$ and Ba $_2$ YMoO $_6$ based cubic double perovskites: an ab initio study, Phys. Scr. 99 (2024) 015908, https://doi.org/10.1088/1402-4896/ad1021.
[36] A.U. Haq, T.S. Ahmad, A. Ahmad, B.S. Almutairi, M. Amin, M.I. Khan, N. Ehsan, R. Sharma, A2LiGaI6 (a = Cs, Rb): new lead-free and direct bandgap halide double perovskites for IR application, Heliyon 9 (2023) e21702, https://doi.org/10.1016/j.heliyon.2023.e21702.
[37] D. Behera, S.K. Mukherjee, Optoelectronics and transport phenomena in Rb2InBiX6 (X = cl, Br) compounds for renewable energy applications: a DFT insight, Chemistry 4 (2022) 1044–1059, https://doi.org/10.3390/chemistry4030071.
[38] S. Iqbal, G.M. Mustafa, M. Asghar, N.A. Noor, M.W. Iqbal, A. Mahmood, Y.-H. Shin, Tuning the optoelectronic and thermoelectric characteristics of narrow bandgap Rb2AlInX6(X= cl, Br, I) double perovskites: a DFT study, Mater. Sci. Semicond. Process. 143 (2022) 106551, https://doi.org/10.1016/j.mssp.2022.106551.
[39] R. Anbarasan, M. Srinivasan, R. Suriakarthick, H. Albalawi, J.K. Sundar, P. Ramasamy, Q. Mahmood, Exploring the structural, mechanical, electronic, and optical properties of double perovskites of Cs2AgInX6 (X = cl, Br, I) by first-principles calculations, J. Solid State Chem. 310 (2022) 123025, https://doi.org/10.1016/j.jssc.2022.123025.
[40] M. Aslam Khan, H.A. Alburaih, N.A. Noor, A. Dahshan, Comprehensive investigation of Opto-electronic and transport properties of Cs2ScAgX6 (X = cl, Br, I) for solar cells and thermoelectric applications, Sol. Energy 225 (2021) 122–128, https://doi.org/10.1016/j.solener.2021.07.026.
[41] A. Ayyaz, G. Murtaza, M. Umer, A. Usman, H.H. Raza, Structural, elastic, optoelectronic, and transport properties of Na-based halide double perovskites Na2CuMX6 (M = Sb, bi, and X = cl, Br) as renewable energy materials: a DFT insight, J. Mater. Res. 38 (2023) 4609–4624, https://doi.org/10.1557/s43578-023-01181-9.
[42] D.-Y. Hu, X.-H. Zhao, T.-Y. Tang, L.-M. Lu, L. Li, L.-K. Gao, Y.-L. Tang, Study on the structural, electronic and optical properties of double-perovskite halides Cs2AgSbX6 (X=I, Br, cl) based on first-principles, Mater. Sci. Semicond. Process. 152 (2022) 107077, https://doi.org/10.1016/j.mssp.2022.107077.
[43] Q. Tang, X. Zhu, Half-metallic double perovskite oxides: recent developments and future perspectives, J. Mater. Chem. C 10 (2022) 15301–15338.
[44] P. Blaha, K. Schwarz, F. Tran, R. Laskowski, G.K.H. Madsen, L.D. Marks, WIEN2k: an APW+lo program for calculating the properties of solids, J. Chem. Phys. 152 (2020) 074101, https://doi.org/10.1063/1.5143061.
[45] J.P. Perdew, K. Burke, M. Ernzerhof, Generalized gradient approximation made simple, Phys. Rev. Lett. 77 (1996) 3865–3868, https://doi.org/10.1103/PhysRevLett.77.3865.
[46] C.G. Broyden, The convergence of a class of double-rank minimization algorithms: 2. The new algorithm, IMA J. Appl. Math. 6 (1970) 222–231.
[47] C. Ambrosch-Draxl, J.O. Sofo, Linear optical properties of solids within the full-potential linearized augmented planewave method, Comput. Phys. Commun. 175 (2006) 1–14.
[48] M.E. Ketfi, S.S. Essaoud, S. Al Azar, A.Y. Al-Reyahi, DFT study of structural, electronic, magnetic and thermodynamic properties of XMnZ2 (X = au, hg, and Tl, Z = S, se) Delafossites, J. Inorg. Organomet. Polym. Mater. (2024), https://doi.org/10.1007/s10904-024-03142-z.
[49] F.D. Murnaghan, The compressibility of media under extreme pressures, Proc. Natl. Acad. Sci. 30 (1944) 244–247, https://doi.org/10.1073/pnas.30.9.244.
[50] S. Sâad Essaoud, A. Bouhemadou, M.E. Ketfi, D. Allali, S. Bin-Omran, Structural parameters, electronic structure and linear optical functions of LuXCo2Sb2 (X = V, Nb and ta) double half Heusler alloys, Phys. B Condens. Matter 657 (2023) 414809, https://doi.org/10.1016/j.physb.2023.414809.
[51] S. Sâad Essaoud, S.M. Al Azar, A.A. Mousa, A.Y. Al-Reyahi, DFT-based investigation of electronic-structure, magnetic and thermoelectric properties of Dy2CoMnO6 double perovskite, Phys. Scr. 98 (2023) 075930.
[52] S.S. Essaoud, A. Bouhemadou, M.E. Ketfi, M. Radjai, D. Allali, DFT+ U based characterization of structural, magnetic, dynamic, elastic and thermodynamic properties of KXF3 (X= Fe or co) halide perovskites compounds, Chem. Phys. Lett. 850 (2024) 141455.
[53] S. Saad Essaoud, A. Bouhemadou, D. Allali, M.E. Ketfi, M. Radjai, S. Bin-Omran, An ab initio investigation of the structural stability, thermodynamic, optoelectronic, and thermoelectric properties of LuXNi2Sn2 (X = V, Nb, ta) double half Heusler materials, J. Inorg. Organomet. Polym. Mater. 34 (2024) 885–902, https://doi.org/10.1007/s10904-023-02881-9.
[54] A.Y. Al-Reyahi, A. Mufleh, S.M. Al Azar, M. Maghrabi, N. Al Aqtash, S.S. Essaoud, K. Berarma, A. Shaheen, M.E. Ketfi, A.A. Mousa, Exploring the physical properties of cubic CsGeBr3-nIn (n= 0, 1, 2, 3) compounds: ab initio calculations of perovskites prospective for the application in solar cells, Solid State Sci. 148 (2024) 107435, https://doi.org/10.1016/j.solidstatesciences.2023.107435.
[55] A. Aqili, A.Y. Al-Reyahi, S.M. Al Azar, S. Saad Essaoud, M. Elamin Ketfi, M. Maghrabi, N. Al Aqtash, A. Mufleh, Investigating the physical characteristics of inorganic cubic perovskite CsZnX3 (X = F, cl, Br, and I): an extensive ab initio study towards potential applications in photovoltaic perovskite devices, Comput. Theor. Chem. 1238 (2024) 114721, https://doi.org/10.1016/j.comptc.2024.114721.